

## STUDY OF IONOSPHERIC EFFECTS ON AZIMUTH IMAGING FOR MEDIUM-EARTH-ORBIT SAR

Liang Li<sup>1, 2, 3, \*</sup> and Jun Hong<sup>1, 2</sup>

<sup>1</sup>Institute of Electronics, Chinese Academy of Sciences, Beijing 100190, China

<sup>2</sup>Sciences and Technology on Microwave Imaging Laboratory, Beijing 100190, China

<sup>3</sup>University of Chinese Academy of Sciences, Beijing 100049, China

**Abstract**—The Medium-Earth-Orbit SAR (MEOSAR) is one of the most potential next-generation spaceborne SARs for its excellent performances. However, the MEOSAR may not be able to produce data useful for science applications due to ionospheric effects. So it is very necessary to study ionospheric effects for the development of MEOSAR. In this paper, we present ionospheric effects on azimuth imaging for MEOSAR. First, we established an analysis model for ionospheric effects on azimuth imaging of MEOSAR based on the system characteristics of MEOSAR and the temporal-variability of ionosphere. Then, based the analysis model, we analyzed the effects caused by the quadratic and cubic phase errors induced by temporal-variability of ionosphere on azimuth imaging. According to the results of our analysis, we conclude that both the quadratic phase error and the cubic phase error being neglected for Low-Earth-Orbit SAR (LEOSAR) will deteriorate the azimuth imaging for MEOSAR. Furthermore, ionospheric effects will become more and more serious with the increase of SAR altitude and the improvement of azimuth resolution designed.

### 1. INTRODUCTION

High resolution and wide swath are our expectation for spaceborne Synthetic Aperture Radar (SAR). However, they are contrary to each other and it is difficult for Low-Earth-Orbit SAR (LEOSAR) to meet

---

*Received 21 May 2013.*

\* Corresponding author: Liang Li (liliang282@163.com).

the both simultaneously. It is an effective method for solving the contradiction through heightening the orbit of SAR, and it is possible for Medium-Earth-Orbit SAR (MEOSAR) and Geosynchronous SAR with the development of the technology in radar. Since the beginning of 21th century, more and more attention has been paid to MEOSAR [1–3]. MEOSAR can vastly improve the performances of LEOSAR and has become one of the important development directions because of its abilities in broad surveillance, imaging with wide swath and high quality, high precision repeat orbit interferometric measurement, rapid response to emergency and so on [4]. Many researchers have studied MEOSAR for synchronization technology, orbit design, performance analysis, imaging process, moving target detection and so on [5–9]. Therefore, we can see that MEOSAR has become one of the most popular spaceborne SAR sensors.

Spaceborne SAR often works above the ionosphere and radio signal will be inevitably affected by the ionosphere, which will cause ionosphere-induced effects such as phase fluctuation, group delay, Doppler frequency-shift, dispersive and Faraday rotation [10, 11]. So the performances of SAR will degrade due to ionospheric effects. Many researchers have studied the ionospheric effects on LEOSAR [12–14], but there are few papers about ionospheric effects on MEOSAR. Only S. H. Hobbs discussed the effects on geosynchronous SAR and L. J. Huang discussed the effects on MEOSAR due to ionospheric perturbations [15, 16].

There are many advantages for MEOSAR. However, the influences on azimuth imaging induced by temporal-variability of ionosphere will be serious with the increase of the synthetic time. In this paper, an analysis model for ionospheric effects on MEOSAR azimuth imaging is established based on the system characteristics of MEOSAR and the temporal-variability of ionosphere, and based the analysis model, the effects caused by the quadratic and cubic phase errors induced by temporal-variability of ionosphere on azimuth imaging are analyzed.

## 2. ANALYSIS ABOUT SPECIFICATIONS OF MEOSAR

The altitude of MEOSAR is between LEOSAR and Geosynchronous SAR. The increase of altitude makes MEOSAR possess a lot of advantages compared to LEOSAR. However, there are many difficulties to face such as system design, imaging process and correction for ionospheric effects. In this section, the dependency relationship between some specifications of MEOSAR and altitude is deduced and analyzed, from which we can see the advantages of MEOSAR.

## 2.1. Range Resolution

Using wide-band signal and pulse compressed technology can improve the resolution in range for SAR. The slant range resolution of SAR sensor, expressed as Equation (1), depends on the signal bandwidth.

$$\rho_r = \frac{c}{2B} \quad (1)$$

where  $\rho_r$  is the slant range resolution,  $B$  is the bandwidth of signal and  $c$  is the velocity of light.

In fact, we want to know the ground range resolution ( $\rho_{gr}$ ) in many applications. Assuming the incidence angle on ground is  $\theta$ , then the ground range resolution can be expressed as Equation (2) [1].

$$\rho_{gr} = \frac{\rho_r}{\sin \theta} \quad (2)$$

From Equation (2), we can see that the ground range resolution will be poor in near range and good in far range for a SAR sensor with a given bandwidth due to the difference of incident angles at the whole swath. D. Bruno et al. [1] pointed out that the change of incidence angles on ground is less for MEOSAR than LEOSAR with the condition that the swath is the same. Therefore, for a given swath, the coincidence in ground range resolution will be better for MEOSAR than for LEOSAR.

## 2.2. Azimuth Resolution

A synthetic aperture can be derived through the movement of antenna, and the higher resolution in azimuth will be obtained. The azimuth resolution  $\rho_a$  can be expressed as Equation (3) [4].

$$\rho_a = \frac{V_g}{B_a} \quad (3)$$

where  $B_a$  is the Doppler bandwidth and  $V_g$  is the velocity of the beam projected on ground.

Assuming inclined angle is  $90^\circ$  and neglecting the rotation of the earth, the velocity of the beam projected on ground at nadir can be estimated from Equation (4).

$$V_N \approx R_e \sqrt{\mu/R_s^3} \quad (4)$$

where  $\mu = 3.986 \times 10^{14} \text{ m}^3/\text{s}^2$  is the gravitation constant of the earth and  $V_N$  is the velocity of the beam projected on ground at nadir.  $R_e$  and  $R_s$  are radiuses of the earth and SAR orbit respectively.

From Equation (4), we can see that  $V_N$  will decrease as SAR altitude increases. So we can derive from Equation (3) that the Doppler

bandwidth needed can be less for MEOSAR than LEOSAR when the azimuth resolution is the same, that is to say, when the Doppler bandwidth is the same, the resolution in azimuth for MEOSAR will be better than LEOSAR.

### 2.3. Swath

The swath of spaceborne SAR is restricted by azimuth resolution, ambiguities of range and azimuth, signal-to-noise ratio etc.. The contradiction between azimuth resolution and swath is an important factor that restricts the performances for LEOSAR. Some advanced techniques are used in antenna to raise swath at present and heightening SAR altitude is another approach to increase swath. Equation (5) gives the inequation for spaceborne SAR system [4].

$$B_a < \text{PRF} < \frac{c}{2S_w} \quad (5)$$

where PRF is the pulse repeated frequency (PRF) and  $S_w$  is the swath of SAR.

As described in the Section 2.2, the Doppler bandwidth needed for MEOSAR can be less than LEOSAR for a given azimuth resolution. So we can know that the PRF can be less for MEOSAR from the left inequation in Equation (5). In addition, with the decrease of PRF, we can conclude from the right inequation in Equation (5) that the swath of SAR can be larger for MEOSAR.

### 2.4. Synthetic Time

It's weel-know that the echo of spaceborne SAR in azimuth is also the linear frequency-modulated signal approximately. The rate of frequency modulated in azimuth at the center of azimuth beam denoted as  $K_a$  can be expressed approximately as Equation (6) [4].

$$K_a = \frac{2V_r^2}{\lambda R_c} \quad (6)$$

where  $V_r \approx \sqrt{V_g V_s}$  is the equivalent velocity and  $V_s = \sqrt{\frac{\mu}{R_s}}$  is the velocity of SAR.  $R_c$  is the range from SAR to the target at the center of azimuth beam.

Combined Equation (3) with Equation (6), we can derive the synthetic time denoted as  $T_a$  described as Equation (7) [4].

$$T_a \approx \frac{\lambda R_c}{2\rho_a V_s} \quad (7)$$

Compared with LEOSAR,  $R_c$  will be larger and  $V_s$  will be smaller, so from Equation (7) we can see that the synthetic time for MEOSAR will be larger than LEOSAR for a given azimuth resolution. Because of the larger synthetic time, the change of ionosphere along with the time must be considered and the degradation in azimuth imaging induced by the temporal variety of ionosphere will be serious accordingly.

### 3. IONOSPHERIC EFFECTS ON PROPAGATION OF SIGNAL

Spaceborne SAR often works above the ionosphere and radio signal will be unavoidably affected by the ionosphere, so ionospheric effects such as phase advance, group delay and dispersion must be taken into consideration.

#### 3.1. Group Delay

The refractive index denoted as  $n$  can be expressed approximately as below according to the theory of Appleton-Hartree [17, 18].

$$n \approx 1 - \frac{\omega_p^2}{2\omega^2} \quad (8)$$

where  $\omega_p = \sqrt{e^2 N_e / m \varepsilon_0}$  is the angular plasma frequency.  $e$  and  $m$  are the charge and mass of an electron respectively.  $\varepsilon_0$  is the electric permittivity of free space,  $N_e$  is the electron density and  $\omega$  is the angular frequency of electromagnetic wave.

The velocity of electromagnetic wave in the ionosphere denoted as  $v_{ion}$  can be expressed as Equation (9).

$$v_{ion} = c \cdot n = c \left( 1 - \frac{\omega_p^2}{2\omega^2} \right) \quad (9)$$

From Equation (9) we can see that the velocity of electromagnetic wave in the ionosphere will decrease, so an extra delay will arise. The two-way extra delay denoted as  $\tau_{gi}$  can be expressed as Equation (10) [17].

$$\tau_{gi} = 2 \frac{\int_s (1 - n) dl}{c} \approx \frac{80.6}{cf^2} \cdot \text{TEC} \quad (10)$$

where  $s$  is the ray path and  $\text{TEC} = \int_s N_e dl$  is the total electron content along the path.  $c$  is the velocity of light and  $f$  is the frequency of electromagnetic wave.

The extra delay induced by ionosphere will introduce a range shift in the focused image for SAR.

### 3.2. Phase Advance

There will be a phase advance for wave propagating in ionosphere because the refractive index in ionosphere is less than one, which will introduce the phase error. The phase advance denoted as  $\phi_{ion}$  induced by ionospheric TEC can be evaluated from Equation (11) [17, 18].

$$\phi_{ion} = -\frac{2\pi \cdot 80.6}{cf} \cdot \text{TEC}_s \quad (11)$$

where  $\text{TEC}_s$  is the total electron content along the path.

The effects of phase error on the image quality depends on both the magnitude and the function form of the phase error. When the quadratic phase error is less than  $\pi/4$  for all the frequencies, the effect on image quality can be ignored [19]. If the phase error is time-invariable and only depends on the frequency, then only the range imaging will be affected. Otherwise, if the phase error is time-dependent, the image quality in azimuth will also be affected.

Because the change of TEC in synthetic time cannot be neglected for MEOSAR, from Equation (11) we can know the phase error induced by ionosphere is not only a function of frequency but also varies with azimuth positions. Therefore, both range imaging and azimuth imaging will be affected by the ionosphere. To emphasize the ionospheric effects due to change of ionosphere during the longer synthetic time for MEOSAR, we will only analyze the influence on azimuth imaging in this paper.

## 4. EFFECTS ON MEOSAR AZIMUTH IMAGING

### 4.1. Model for Analysis

The ideal SAR echo can be expressed as Equation (12).

$$s_0(\tau, \eta) = A_0 \cdot \exp \left\{ -j \frac{4\pi f_0 R(\eta)}{c} \right\} \cdot \exp \left\{ j\pi k_r (\tau - 2R(\eta)/c)^2 \right\} \quad (12)$$

where  $\tau$  is the fast time and  $\eta$  is the slow time.  $A_0$  denotes the amplitude and  $k_r$  is the rate of frequency modulated.  $f_0$  is the center frequency operated and  $R(\eta)$  is the distant from SAR to target at the time of  $\eta$ .

Considering the group delay and phase advance induced by ionosphere, Equation (12) can be expressed as Equation (13).

$$\begin{aligned} s_{0\_ion}(\tau, \eta) = A_0 \cdot \exp \left\{ -j \frac{4\pi f_0 R(\eta)}{c} \right\} \cdot \exp \left\{ j\pi k_r \tau_{ion}^2 \right\} \\ \cdot \exp \left\{ j\phi_{ion}(f, \eta) \right\} \end{aligned} \quad (13)$$

where  $\tau_{ion} = \tau - 2R(\eta)/c - \tau_{gi}$ .

For SAR sensor, TEC is a function of slow time in azimuth. A Taylor expansion about TEC at  $\eta = 0$  is performed and Equation (14) can be derived [13]:

$$\begin{aligned} \text{TEC}_s(\eta) = & \text{TEC}_s(0) + \text{TEC}'_s(0) \cdot \eta + \frac{\text{TEC}''_s(0)}{2} \cdot \eta^2 \\ & + \frac{\text{TEC}'''_s(0)}{6} \cdot \eta^3 + \dots \end{aligned} \quad (14)$$

where  $\text{TEC}(0)$  is the TEC at  $\eta = 0$ .  $\text{TEC}'(0)$ ,  $\text{TEC}''(0)$  and  $\text{TEC}'''(0)$  are one-order, two-order and three-order derivatives of TEC respectively.

From Equation (14) we can see that the phase errors induced by ionospheric TEC include constant error, linear error, quadratic error, cubic and high-order phase error. The first two terms don't impact the image quality. The quadratic phase error will cause mainlobe to widen and sidelobes to rise, and the cubic phase error will induce an asymmetrical distortion in azimuth image. The high-order error is usually small and can be neglected.

For LEOSAR, synthetic time is usually less than one second, so ionospheric TEC can be considered as constant during the synthetic time and the effects induced by background ionosphere can be ignored. However, synthetic time increases a lot for MEOSAR, so the phase error induced by ionosphere will increase accordingly. In this section, only the ionospheric effects induced by the quadratic and cubic phase errors are considered and analyzed.

## 4.2. Simulation

For MEOSAR, both synthetic time and synthetic aperture increase a lot compared to LEOSAR, so the variance of TEC in the synthetic time cannot be neglected. And the quadratic and cubic phase errors induced by temporal-variability of ionospheric TEC will affect the azimuth imaging. In this section, the quadratic and cubic phase errors induced by ionosphere are analyzed when SAR altitudes are 600 km, 1300 km, 3000 km and 10000 km respectively. The parameters for simulation are listed in Table 1.

### 4.2.1. Effect Induced by Quadratic Phase Error

Combining Equation (11) with Equation (14), we can calculate the quadratic phase error in azimuth induced by TEC. It is expressed as

**Table 1.** Parameters of SAR for simulation.

Altitude (km)	600	1300	3000	10000
Frequency (GHz)	1.25	1.25	1.25	1.25
Azimuth Resolution (m)	5	5	5	5
Synthetic Time (s)	2.6	5.7	13.7	54.5
Doppler Bandwidth (Hz)	1384	1198	890	400
Slant Angle (°)	0	0	0	0
Scene Incidence Angle (°)	45	45	45	45
Look Angle (°)	40.2	36.0	28.7	16.0
$d^2 \text{TEC}/dt^2$	0.01 TEC <sub>u</sub>	0.01 TEC <sub>u</sub>	0.01 TEC <sub>u</sub>	0.01 TEC <sub>u</sub>
$d^3 \text{TEC}/dt^3$	0.003 TEC <sub>u</sub>	0.003 TEC <sub>u</sub>	0.003 TEC <sub>u</sub>	0.003 TEC <sub>u</sub>

**Table 2.** Effects on resolution and PSLR caused by quadratic phase error.

SAR Altitude		600 km	1300 km	3000 km	10000 km
Resolution/m		4.72	5.24	18.38	657.22
PSLR/dB	Left	13.45	12.98	9.02	/
	Right	13.45	12.98	9.02	/

Equation (15).

$$\Phi_2 = -\frac{\pi \cdot 80.6}{cf_0} \cdot \text{TEC}_s'' \eta^2 \quad (15)$$

Assuming the ionospheric state is the same, the longer synthetic time for MEOSAR will introduce a larger peak quadratic phase error. Therefore, the azimuth imaging will be affected more significantly. Figure 1 gives the simulation results of image in azimuth that are affected by the quadratic phase error, and Table 2 quantificationally presents the degradation in PSLR and resolution caused by the quadratic phase error. It can be seen from Figure 1 and Table 2 that the degradation of the image quality in azimuth caused by the quadratic phase error becomes more and more obviously with the increase of orbit on condition of the same ionosphere state for L-band SAR sensor.

#### 4.2.2. Effect Induced by Cubic Phase Error

For LEOSAR, the cubic phase error is not generally considered, but the cubic phase error will increase a lot with the increase of synthetic



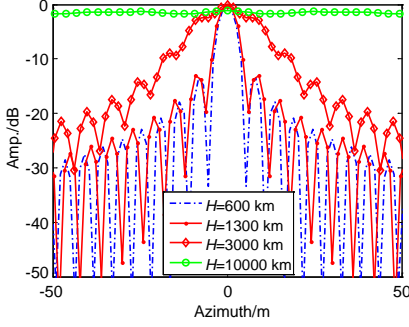


**Figure 1.** Distortion caused by quadratic phase error in azimuth image.

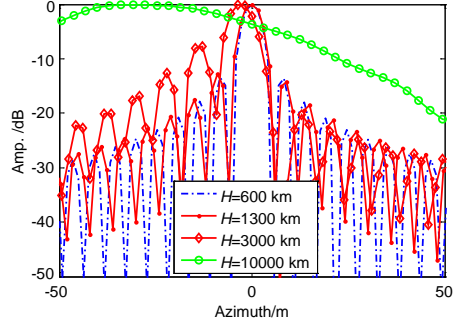


**Figure 2.** Distortion caused by cubic phase error in azimuth image.

**Table 3.** Effects of resolution and PSLR caused by cubic phase error.

SAR Altitude		600 km	1300 km	3000 km	10000 km
Resolution/m		4.72	5.23	6.61	46.08
PSLR/dB	Left	13.40	12.78	7.41	2.08
	Right	13.54	14.06	20.35	32.48

time for MEOSAR. From Equation (11) and Equation (14), we can calculate the cubic phase error in azimuth induced by TEC, which is expressed as Equation (16).

$$\Phi_3 = -\frac{\pi \cdot 80.6}{3 \cdot c f_0} \cdot \text{TEC}_s''' \cdot \eta^3 \quad (16)$$

Figure 2 gives the simulation results of image in azimuth affected by the cubic phase error, and Table 3 quantificationally presents the degradation in PSLR and resolution caused by the cubic phase error. It can be seen from Figure 2 and Table 3 that the degradation of the image quality in azimuth caused by the cubic phase error becomes more and more dominantly with the increase of orbit on condition of the same ionosphere state for L-band SAR sensor.

#### 4.2.3. Relation between Effects Induced by Ionosphere and Resolution

The peak quadratic phase error denoted as  $\phi_{2a}$  and cubic phase error denoted as  $\phi_{3a}$  can be derived from Equation (15) and Equation (16).

$$\phi_{2a} = -\frac{2\pi \cdot 80.6}{c f_c} \cdot \frac{\text{TEC}_s''}{2} \cdot (T_a/2)^2 \quad (17)$$

$$\phi_{3a} = -\frac{2\pi \cdot 80.6}{c f_c} \cdot \frac{\text{TEC}_s'''}{6} \cdot (T_a/2)^3 \quad (18)$$

where  $T_a$  is the synthetic time.

The azimuth resolution can also be expressed as Equation (19).

$$\rho_a = \frac{\lambda R_0}{2L_s} \quad (19)$$

where  $R_0$  is the centre range,  $L_s = v_s \cdot T_a$  is the synthetic aperture and  $v_s = \sqrt{\mu/R_s}$  is the velocity of SAR.  $R_s$  is the radius of the orbit.  $\mu = 3.986 \times 10^{14} \text{ m}^3/\text{s}^2$  is the gravitation constant of the earth.

The effects induced by the quadratic phase error can be ignored when  $\phi_{2a}$  is smaller than  $\pi/4$  [19], so if Equation (20) is satisfied, the effects induced by the quadratic phase error can be ignored.

$$\phi_{2a} = -\frac{2\pi \cdot 80.6}{cf_c} \cdot \frac{\text{TEC}_s''}{2} \cdot (T_a/2)^2 < \frac{\pi}{4} \quad (20)$$

Combining Equation (20) with Equation (19), Equation (21) can be obtained.

$$\rho_a^2 > \frac{80.6 \cdot \lambda^2 \cdot \text{TEC}_s'' \cdot R_0^2 \cdot R_s}{4\mu \cdot c \cdot f_c} \quad (21)$$

Equation (21) gives the relationship between the azimuth resolution and the two-order derivative of TEC when the effect on azimuth resolution induced by ionospheric quadratic phase error can be ignored.

Furthermore, the effects on resolution induced by the cubic phase error can be ignored when  $\phi_{3a}$  is smaller than  $\pi/2$ . Similarly to analyze on the quadratic phase error, the relationship between the azimuth resolution and the third-order derivative of TEC can be expressed as Equation (22) when the effect on azimuth resolution induced by ionospheric cubic phase error can be ignored.

$$\rho_a^3 > \frac{80.6 \cdot \lambda^3 \cdot \text{TEC}_s''' \cdot R_0^3}{96c \cdot f_c \cdot (\mu/R_s)^{3/2}} \quad (22)$$

To analyze the relationship between the effects on the image quality induced by TEC variety with the resolution, a computational simulation model is developed to describe azimuth imaging affected by the quadratic phase error and cubic phase error induced by TEC variety when the height of orbit is 3000 km and the resolution changes from 5 m to 100 m. Other parameters used in the simulation are shown in Table 1. The simulation results are shown in Figure 3 and Figure 4. It can be seen from Figure 3 and Figure 4 that the higher the resolution is, the more significantly the effects on azimuth imaging induced by the temporal-variety of ionosphere are. For given parameters used in the simulation, when the azimuth resolution is 5 m, the azimuth imaging

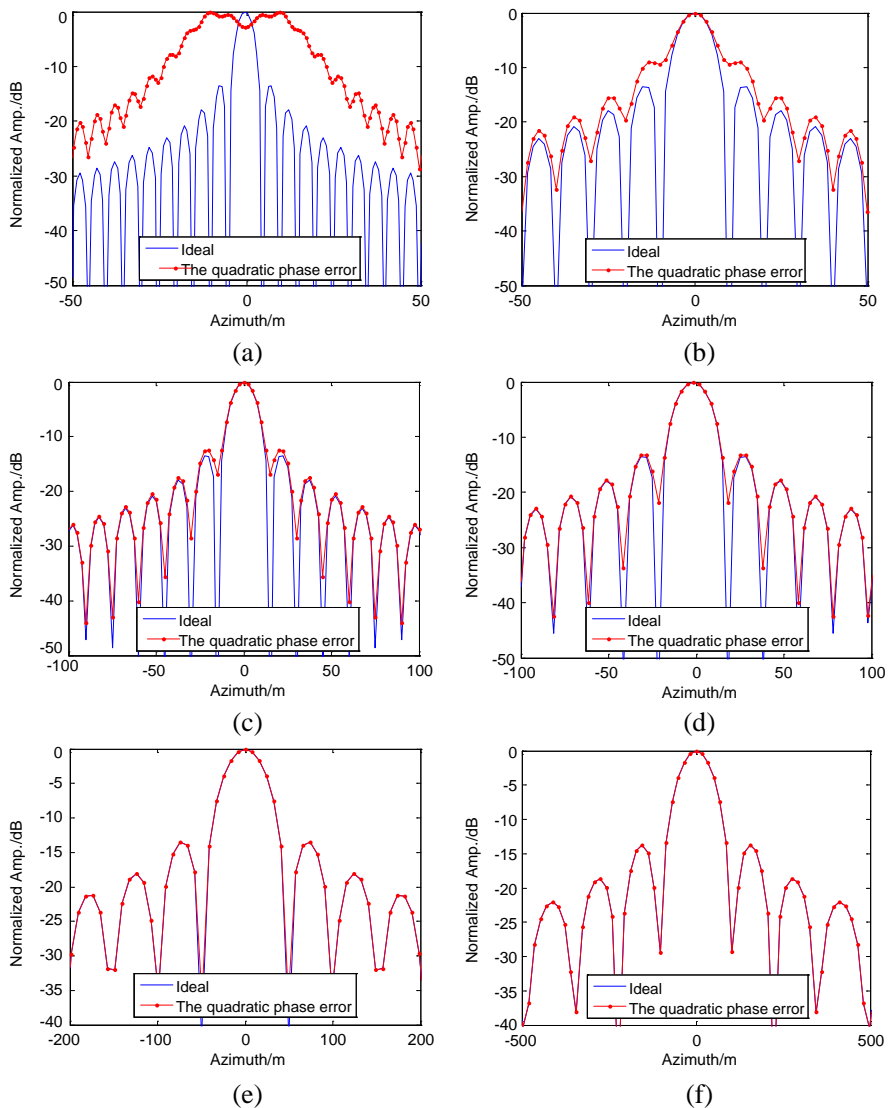


**Figure 3.** The results of image in azimuth affected by quadratic phase error for various resolutions. (a)  $\rho_a = 5$  m. (b)  $\rho_a = 10$  m. (c)  $\rho_a = 15$  m. (d)  $\rho_a = 20$  m. (e)  $\rho_a = 50$  m. (f)  $\rho_a = 100$  m.

is badly affected by the quadratic phase error. However, when the resolution exceeds 15 m, the effect induced by the quadratic phase error is small and can be ignored. With regard to the cubic phase error, the cubic phase error will barely affect the resolution of azimuth

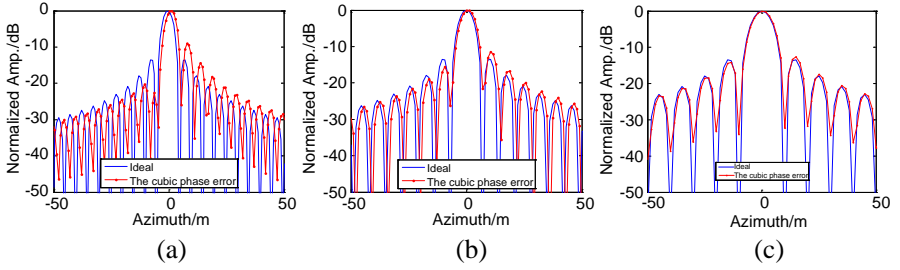


**Figure 4.** The results of image in azimuth affected by cubic phase error for various resolutions. (a)  $\rho_a = 5$  m. (b)  $\rho_a = 7$  m. (c)  $\rho_a = 10$  m.

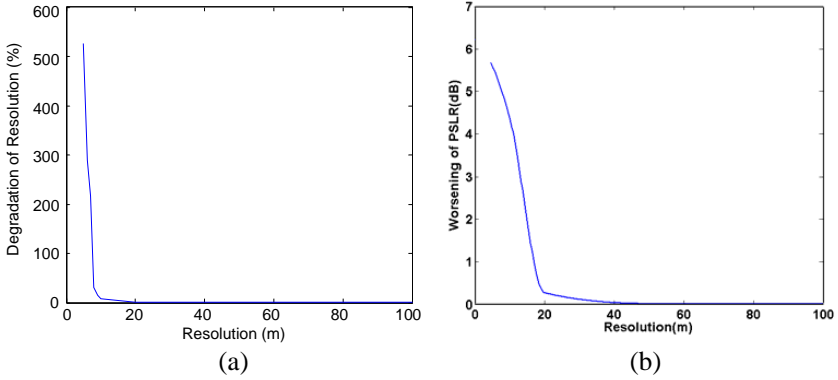


**Figure 5.** Worsening of resolution and PSLR vs. resolution. (a) Resolution. (b) PSLR.

image when the resolution is 5 m. Meanwhile, the effects on the quality in azimuth image can be ignored when the resolution is bigger than 7 m. These conclusions also can be derived from Equation (21) and Equation (22), which shows that the results from simulation are in accordance with the theoretically analyzing.

In order to show the effects on azimuth imaging induced by ionospheric phase error intuitively, Figure 5 gives the changes of degradation in azimuth resolution and PSLR vs. resolution. It can be seen from Figure 5 that the higher the azimuth resolution is, the more significant the effects on azimuth image quality induced by TEC variety are. From the analysis above, we can see that the effects on image quality in azimuth induced by ionospheric TEC variety are significant for MEOSAR, especially for high resolution MEOSAR. Therefore, proper measures should be taken to mitigate ionospheric effects for MEOSAR.

## 5. CONCLUSION

In this paper, the model for analyzing ionospheric effects on MEOSAR is established. Based on the model, we analyzed the influences on L-band MEOSAR azimuth imaging caused by ionosphere-induced phase errors. The results of simulations show that the quadratic and cubic phase errors neglected for LEOSAR will introduce a significant distortion in azimuth image for MEOSAR. Moreover, the ionospheric effect becomes more and more significant with the increase of SAR altitude and the improvement of azimuth resolution. So measures must be taken to correct the ionospheric effect especially for low-frequency and high-resolution MEOSAR.

## REFERENCES

1. Bruno, D., S. Hobbs, and G. Ottavianelli, "Geosynchronous synthetic aperture radar: Concept design, properties and possible applications," *Acta Astronautica*, Vol. 59, 149–156, 2006.
2. Yu, Z., et al., "Concepts, properties and imaging technologies for GEO SAR," *Proceedings of SPIE*, Vol. 7494, 749407/1–749407/8, 2009.
3. Edelstein, W., S. Madsen, A. Moussessian, and C. Chen, "Concepts and technologies for synthetic aperture radar from MEO and geosynchronous orbits," *Proceedings of SPIE*, Vol. 5659, 195–203, Bellingham, USA, 2005.
4. Huang, L. J., "Imaging algorithm for Medium-Earth-Orbit SAR," Ph.D. Thesis, Institute of Electronics, Chinese Academy of Sciences, 2010.
5. Liu, Q., W. Hong, W. X. Tan, Y. Lin, Y. Wang, and Y. Wu, "An improved polar format algorithm with performance analysis for geosynchronous circular SAR 2D imaging," *Progress In Electromagnetics Research*, Vol. 119, 155–170, 2011.
6. Zheng, J. B., H. J. Song, X. Q. Shang, et al., "Doppler properties analysis of GEO spaceborne SAR," *Journal of Electronics & Information Technology*, Vol. 33, 810–815, 2011.
7. Liu, Q., W. Hong, W. X. Tan, and Y. Wu, "Efficient geosynchronous circular SAR raw data simulation of extended 3-D scenes," *Progress In Electromagnetics Research*, Vol. 127, 335–350, 2012.
8. Bao, M., M. D. Xing, Y. Wang, and Y. C. Li, "Two-dimensional spectrum for MEO SAR processing using a modified advanced

- hyperbolic range equation,” *Electronics Letters*, Vol. 47, No. 18, 1043–1045, 2011.
9. Hu, C., T. Long, and Y. Tian, “An improved nonlinear chirp scaling algorithm based on curved trajectory in geosynchronous SAR,” *Progress In Electromagnetics Research*, Vol. 135, 481–513, 2013.
  10. Chaudhary, K. and B. R. Vishvakarma, “Effect of ionospheric induced depolarization on satellite solar power station,” *Progress In Electromagnetics Research Letters*, Vol. 9, 39–47, 2009.
  11. Chen, J., S. Quegan, and X. Yin, “Calibration of spaceborne linearly polarized low frequency SAR using polarimetric selective radar calibrators,” *Progress In Electromagnetics Research*, Vol. 114, 89–111, 2011.
  12. Tsynkov, S. V., “On SAR imaging through the Earth’s ionosphere,” *SIAM J. Imaging Sci.*, Vol. 2, 140–182, 2009.
  13. Kim, Y. J. and J. van Zyl, “Ionospheric effects on polarimetric and interferometric space-borne SAR,” *IGARSS 1998*, Vol. 1, 472–474, 1998.
  14. Li, L. L., “Spaceborne SAR signals propagation in the ionosphere and ionosphere image by spaceborne SAR,” Ph.D. Thesis, Institute of Electronics, Chinese Academy of Sciences, 2006.
  15. Bruno, D. and S. E. Hobbs, “Radar imaging from geosynchronous orbit: Temporal decorrelation aspects,” *IEEE Transactions on Geoscience and Remote Sensing*, Vol. 48, No. 7, 2924–2929, 2010.
  16. Huang, L. J., B. Han, D. H. Hu, et al., “Medium-earth-orbit SAR imaging based on keystone transform and azimuth perturbation,” *IGARSS 2012*, 3608–3610, Munich, 2012.
  17. Li, L., J. Hong, F. Ming, et al., “An approach for ionospheric effects correction on spaceborne SAR calibration based on active radar calibrator,” *Journal of Electronics & Information Technology*, Vol. 34, 1096–1101, 2012.
  18. Yesil, A., M. Aydogdu, and A. G. Elias, “Reflection and transmission in the ionosphere considering collisions in a first approximation,” *Progress In Electromagnetics Research Letters*, Vol. 1, 93–99, 2008.
  19. Papathanassiou, K., J. S. Kim, S. Quegan, et al., “Study of ionospheric mitigation schemes and their consequences for BIOMASS product quality,” University of Sheffield, ESA/ESTEC Contract No. 22849/09/NL/JA/ef., European Space Agency, 2012.